Site-Specific Metal Chelation Facilitates the Unveiling of Hidden Coordination Sites in an Fe II/Fe III -Seamed Pyrogallol[4]arene Nanocapsule

Site-Specific Metal Chelation Facilitates the Unveiling of Hidden Coordination Sites in an Fe^{II}/Fe^{III}-seamed Pyrogallol[4]arene Nanocapsule

Asanka S. Rathnayake,[†] Hector W. L. Fraser,[‡] Euan K. Brechin,[‡] Scott J. Dalgarno,[§] Jakob E. Baumeister,[†] Joshua White,[†] Pokpong Rungthanaphatsophon,[†] Justin R. Walensky,[†] Steven P. Kelley,[†] Charles L. Barnes,[†] and Jerry L. Atwood.[*†]

[†]Department of Chemistry, University of Missouri, 601, S. College Avenue, Columbia, MO 65211 (USA)

[‡]EaStCHEM School of Chemistry, The University of Edinburgh, David Brewster Road, EH9 3FJ, Edinburgh (UK)

[§]Institute of Chemical Sciences, Heriot-Watt University, Riccarton, Edinburgh, EH14 4AS (UK)

Supporting Information Placeholder

ABSTRACT: Under suitable conditions, *C*-alkylpyrogallol[4]arenes (PgCs) arrange into spherical metal-organic nanocapsules (MONCs) upon coordination to appropriate metal ions. Herein we present the synthesis and structural characterization of a novel Fe^{II}/Fe^{III}-seamed MONC, as well as studies related to its electrochemical and magnetic behaviors. Unlike other MONCs which are assembled through 24 metal ions, this nanocapsule comprises 32 Fe ions, uncovering 8 additional coordination sites situated between the constituent PgC sub-units. The Fe^{II} ions are likely formed by the reducing ability of DMF used in the synthesis, representing a novel synthetic route towards polynuclear mixed-valence MONCs.

The design of metal-organic supramolecular structures with well-defined shapes and dimensions continues to attract intense interest, a primary reason being their ability to mimic biologically active sites.[1-8] These inorganic-organic hybrids are typically formed by the metal-directed assembly of suitably functionalized organic ligands,[9-17] and recent years have witnessed the synthesis of such species with paramagnetic metal ions; this is a popular strategy due to the inherent potential for one to control or influence the resulting magnetic properties of a system.[9,18-24] Our efforts to synthesize such supramolecular hybrids primarily utilize *C*-alkylpyrogallol[4]arenes (PgC_n, where *n* is the number of carbon atoms in pendant alkyl chains) as organic ligands. Having upper-rim phenolic groups and an associated bowl conformation, coordination to appropriate metal ions can, under appropriate conditions, drive PgC_ns to form a diverse range of metal-PgC_n assembly types.[10,25-32] We are specifically interested in MONCs that typically exist in two general forms, termed hexamers (Figure 1a) and dimers hereafter.[10,25-31] These hexamers and dimers are nanoscale capsules containing either 6 or 2 PgC_n units, and are formed through coordination to 24 or 8 divalent metal ions, respectively. To date we have reported the synthesis and structural characterization of MONCs formed through coordination to different metal ions. Recently, we discovered a novel route to synthesize mixed-valence MONCs through *in-situ* redox chemistry.[33,34] This prompted us to investigate different reaction conditions that may promote the formation of other mixed-valence MONCs. Here we present the synthesis and characterization of an iron-based mixed-valence MONC of formula $[Fe^{II}_{16}Fe^{III}_{16}(PgC_6)_6(Cl)_{16+n}(DMF)_{12}(H_2O)_{20-n}]$ ($n = 0 – 8$) (**1**) (Figure 1b), and, notably, this MONC assembled with 32 metal centers, unveiling 8 additional coordination sites that are located between framework PgC_6 ligands. This spectacular new capsule is also formed through *in-situ* redox reactions, but, most importantly, displays new structural characteristics that are previously unseen for this assembly type; specific chelating sites tend to coordinate with Fe ions with specific oxidation states and the constituent Fe ions exhibit clearly defined coordination patterns that are unique to each oxidation state.

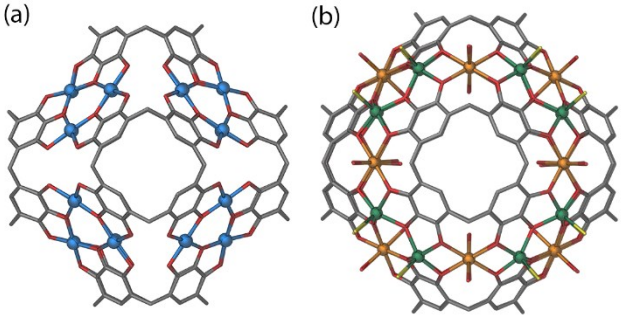

Figure 1. (a) Side view of Cu^{II}-seamed MONC, which represents the metal-ligand arrangement of a typical hexameric MONC, showing 24 coordination sites between constituent PgC sub-units. The Cu^{II} ions coordinate with PgC units in such a way to form 8 $[Cu_3O_3]$ units that cover facets of the MONC. (b) Symmetry expanded single crystal X-ray structure of **1** which is assembled through 32 Fe ions. The additional 8 Fe centers are coordinated such that to bridge / connect neighboring $[Fe_3O_3]$ units. PgC alkyl chains and H atoms omitted for clarity. Color code: Cu^{II} – azure, Fe^{II} – orange, Fe^{III} – green, Cl – yellow, O – red, C – gray.

Nanocapsule **1** was synthesized by reacting PgC_6, $FeCl_3$, and sodium methoxide in a DMF/methanol mixture (Experimental S1 – S3). Slow evaporation of the mother liquor afforded dark blue single crystals that were suitable for diffraction studies over a period of ~10 weeks. Compound **1** crystallized in the monoclinic space

group $P2_1/n$. As can be seen in Figures 1 – 3, the overall structure comprises 6 PgC_6 sub-units and 32 Fe centers, the asymmetric unit consisting of one half of the capsule. Inspection of the structure of **1** readily reveals that, by coordinating to upper-rim PgC_6 units, 24 of the 32 Fe centers are arranged as eight $[Fe_3O_3]$ units. The remaining 8 Fe centers were found to seam the framework in such a way as to bridge adjacent $[Fe_3O_3]$ units; 4 of these 8 Fe centers link four $[Fe_3O_3]$ units, twice, forming two clearly defined metallic hemispheres as a result (Figure S1). All the iron centers are in one of two distinct coordination geometries: distorted square pyramidal geometry or distorted octahedral geometry (Figure S2). By considering both bond-valence sum (BVS) analysis[35] and Fe—O equatorial bond distances, it has been determined that Fe ions in square pyramidal sites are in the 3+ oxidation state, whilst those in octahedral sites are in the 2+ oxidation state (Table S1). With respect to the coordination spheres, each Fe^{III} ion coordinates to four upper-rim phenolic groups equatorially and an axial Cl^- ion on the capsule exterior; this coordination sphere closely resembles that found in a [Fe^{III}-salen] complex.[36-38] In contrast, all Fe^{II} ions in octahedral sites are bonded to four upper-rim phenolic groups, one solvent molecule on the capsule exterior, and an encapsulated water ligand. As shown in Figure 2a, each $[Fe_3O_3]$ unit consists of two Fe^{III} ions (Fe6, Fe14 and equivalents) and one Fe^{II} ion (Fe5 and equivalents), while all bridging sites are occupied by Fe^{II} ions (Fe7 and equivalents). Interestingly, the Fe^{II} ions in each $[Fe_3O_3]$ unit are arranged in such a way to line-up with the outline of each hemisphere, such that no Fe^{II} ions are located adjacent each other (Figure 2b). The interior water ligands of the peripheral Fe5 sites are observed to be disordered with Cl^- ligands with an average of approximately two Cl^- ions per molecule. In order to maintain the charge balance, we believe that, these Cl^- ions abstract protons from the solution (pH = 3.25).

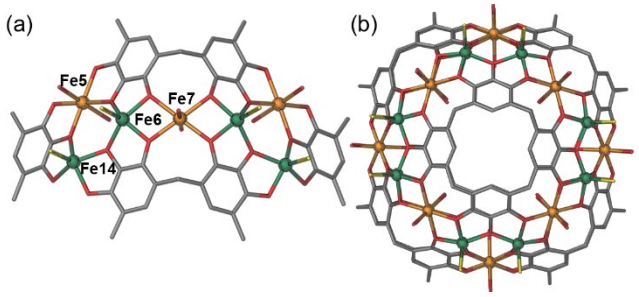

Figure 2. Arrangement of Fe^{II} and Fe^{III} ions on the framework of **1**. (a) Two $[Fe_3O_3]$ units connected through a bridging Fe^{II} ion (Fe7), and (b) arrangement of Fe^{II} ions along the metal-organic hemispheres. PgC_6 alkyl chains and H atoms omitted for clarity. Color code: Fe^{II} – orange, Fe^{III} – green, Cl – yellow, O – red, C – gray.

Most hexameric MONCs reported to date have been constructed through the assembly of 24 metal ions and, with 32 metal centers, compound **1** displays the highest metal ion content in a PgC_n-based MONC. The use of 8 additional coordination sites within the MONC framework suggests that bridging Fe^{II} ions are large enough to fit in between adjacent PgC_6 units without hindering the self-assembly process, albeit that they sit slightly out of the polyphenolic plane. Interestingly, the reaction conditions used here are similar to those of the previously reported [$Co^{II}_{24}(PgC_5)_6$] MONC (Figure S3).[39] However, different structural features exhibited by these two MONCs suggest not only that small changes in reaction conditions may yield MONCs with remarkable features, but also that much remains to be discovered in this burgeoning area of research. Site-specific reactions have been studied as a tool to modify the functionality of nanoscale clusters.[40-42] Similarly, although challenging, directing metal ions into fixed binding sites might be a potential approach to facilitate the fine-tuning of functionality / properties of a metal-organic complex.[40,43] Considering that Fe^{III} and Fe^{II} ions are bonded to specific coordination sites, without altering the main framework, and that site-specific metal chelation is solely promoted by serendipitous assembly, make **1** a landmark polymetallic cage complex.[44]

As outlined above, the structure of **1** reveals the presence of two metal-seamed hemispheres that stitch together through 12 hydrogen bonding interactions (Figure 3a). Interestingly, four of these interactions are located within the cavity and are formed between internal water ligands at the edges of opposing hemispheres (O···O distances in the range of 2.920-2.990 Å, Figures 3b & 3c). These are unique non-covalent interactions for this system type, as a MONC is typically held together by 24 inter- / intramolecular hydrogen bonding interactions between upper-rim phenolic groups (Figure S4). The internal volume of **1**, calculated by using MSroll with a sphere radius of 1.25 Å, was found to be ~1470 Å³. It is clear that the larger void space in **1** (relative to typical MONCs: [$Cu^{II}_{24}(PgC_3OH)_6$] ~1250 Å³, [$Mn^{II}_{24}(PgC_5)_6$] ~1300 Å³, [$Co^{II}_{24}(PgC_5)_6$] ~1400 Å³) is due to expansion of the entire framework that has been invoked by the additional bridging Fe^{II} ions.[30,33,39]

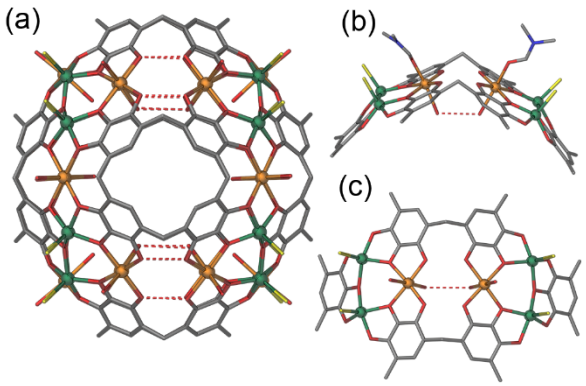

Figure 3. (a) Side view of **1** showing hydrogen bonding interactions between two hemispheres. (b) Side, and (c) top-down views of hydrogen bonding interactions formed between interior axial ligands in opposing hemispheres. PgC_6 alkyl chains and H atoms omitted for clarity. Color code: Fe^{II} – orange, Fe^{III} – green, Cl – yellow, N – blue, O – red, C – gray.

Considering that the framework of **1** consists of both Fe^{II} and Fe^{III} ions, and as only Fe^{III} ions have been used as the starting material, an apparent reduction has taken place during the self-sorting process. This Fe^{III} to Fe^{II} reduction has likely been promoted by the reducing ability of DMF upon hydrolysis (Eq. 1).[45-47] According to the proposed electron transfer reaction, DMF serves as both the reaction medium and reducing agent in the synthesis of **1**.[48]

$$HCON(CH_3)_2 + 2\,Fe^{III} + 3\,H_2O \rightarrow 2\,Fe^{II} + (CH_3)_2NCOOH + 2\,H_3O^+ \qquad (1)$$

The electrochemical activity of Fe^{II}/Fe^{III} mixed-valence centers in complex **1** was analyzed by cyclic voltammetry in acetonitrile with tetraethylammonium perchlorate (TEAP) as the supporting electrolyte in the potential range -1.5 to +1.2 V vs SCE. Two overlapping quasi-reversible reduction waves are seen in this potential range as cathodic peaks (Figure 4). The peak at -0.333 V is consistent with the reduction of Fe^{III} to Fe^{II} and that at the -0.703 V was assigned to the reduction of Fe^{II} to Fe^{I}.[49,50] The observed irreversibility may be due to structural changes in the complex accompanying the redox processes.

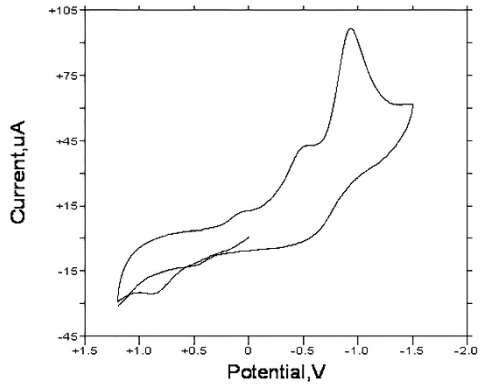

Figure 4. Cyclic voltammogram of **1** in CH_3CN (0.1M TEAP supporting electrolyte, platinum disk working electrode, platinum wire auxiliary electrode) under argon at 100 mV/s, with three successive scans.

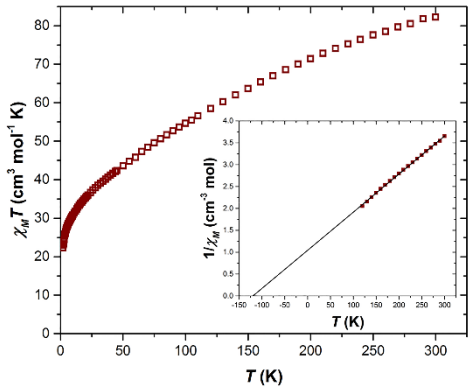

Figure 5. Plot of the $\chi_M T$ product versus T for compound **1**. Inset: plot of $1/\chi_M$ versus T. The solid line is a fit of the data to the Curie-Weiss Law.

DC magnetic susceptibility measurements were carried out on a powdered polycrystalline sample of compound **1** in an applied magnetic field of $H = 0.1$ T over the temperature range $T = 2 – 300$ K. Figure 5 shows the experimental data plotted as the $\chi_M T$ product versus T, where χ_M is the molar magnetic susceptibility. The value of $\chi_M T$ at $T = 300$ K is approximately 83 cm^3 K mol^{-1}, somewhat lower than that expected for the sum of the Curie constants for 16 non-interacting (high-spin octahedral) Fe^{II} ($s = 2$) ions and 16 non-interacting (high-spin square pyramidal) Fe^{III} ($s = 5/2$) ions, with $g = 2.00$ (118 cm^3 K mol^{-1}). As the temperature decreases, the magnitude of $\chi_M T$ decreases steadily, reaching a value of 22.30 cm^3 K mol^{-1} at $T = 2$ K. This behavior indicates the presence of antiferromagnetic (AF) exchange interactions between the constituent metal ions, as would be expected for a large cluster containing multiple O-bridged Fe^{II} and Fe^{III} ions.[51,52] The large nuclearity of the cage and the number of unique exchange interactions prohibits any detailed quantitative analysis of the data, however a fit of the linear section of the $1/\chi_M$ versus T data (Figure 5 inset, 300 – 120 K) affords Curie and Weiss constants of $C = 114.94$ cm^3 K mol^{-1} and $\theta = -119.92$ K, respectively. Magnetization data collected for **1** in the $H = 0 – 7$ T field range at temperatures between $T = 2 – 7$ K are consistent with the presence of AF exchange, the value of M increasing in a near linear-like fashion with increasing H, without reaching saturation (Figure S5).

In conclusion, we have presented the synthesis and structural characterization of the first Fe-seamed PgC_n-based MONC. The framework of this nanocapsule consists of 32 metal centers, uncovering 8 additional coordination sites between the PgC_n sub-units in previously reported MONCs. The Fe ions coordinating the framework are in two different oxidation states, suggesting an occurrence of a reductive process during self-assembly. This reduction of Fe^{III} to Fe^{II} has apparently been facilitated by the reducing ability of DMF upon hydrolysis and, overall, the formation of this polynuclear cage compound has opened a new pathway to the synthesis of polynuclear mixed-valence complexes. Future studies in this area will be focused on investigating different reaction conditions that aid the formation of such types of mixed-valence complexes and synthesizing analogous MONCs with disparate metal ions.

ASSOCIATED CONTENT

Supporting Information

The Supporting Information is available free of charge on the ACS Publications website. X-ray crystallography data for nanocapsules **1** (CCDC 1817707) (CIF). Experimental S1-S3, Table S1, Figures S1-S5 (PDF).

AUTHOR INFORMATION

Corresponding Author

atwoodj@missouri.edu

Author Contributions

The manuscript was written through contribution of all authors. All authors have given approval to the final version of the manuscript.

Notes

The authors declare no competing financial interests.

ACKNOWLEDGMENT

The authors thank the University of Missouri Fellowship Program in Radiochemistry sponsored by US Nuclear Regulatory Commission (NRC) Grant NRC-HQ-84-15-G-0036 (J. E. Baumeister).

REFERENCES

(1) Devereux, M.; Shea, D. O.; Kellett, A.; McCann, M.; Walsh, M.; Egan, D.; Deegan, C.; Kędziora, K.; Rosair, G.; Müller-Bunz, H. Synthesis, X-ray crystal structures and biomimetic and anticancer activities of novel copper (II) benzoate complexes incorporating 2-(4′-thiazolyl) benzimidazole (thiabendazole), 2-(2-pyridyl) benzimidazole and 1, 10-phenanthroline as chelating nitrogen donor ligands. *J. Inorg. Biochem.* **2007**, *101*, 881.

(2) Feng, D.; Gu, Z. Y.; Li, J. R.; Jiang, H. L.; Wei, Z.; Zhou, H. C. Zirconium-metalloporphyrin PCN-222: mesoporous metal–organic frameworks with ultrahigh stability as biomimetic catalysts. *Angew. Chem.* **2012**, *124*, 10453.
(3) Katz, M. J.; Mondloch, J. E.; Totten, R. K.; Park, J. K.; Nguyen, S. T.; Farha, O. K.; Hupp, J. T. Simple and compelling biomimetic metal–organic framework catalyst for the degradation of nerve agent simulants. *Angew. Chem. Int. Ed.* **2014**, *53*, 497.
(4) Kluwer, A.; Kapre, R.; Hartl, F.; Lutz, M.; Spek, A.; Brouwer, A.; Van Leeuwen, P.; Reek, J. Self-assembled biomimetic [2Fe_2S]-hydrogenase-based photocatalyst for molecular hydrogen evolution. *Proc. Natl. Acad. Sci. U.S.A.* **2009**, *106*, 10460.
(5) Rebouças, J. S.; Spasojević, I.; Batinić-Haberle, I. Pure manganese (III) 5, 10, 15, 20-tetrakis (4-benzoic acid) porphyrin (MnTBAP) is not a superoxide dismutase mimic in aqueous systems: a case of structure–activity relationship as a watchdog mechanism in experimental therapeutics and biology. *JBIC, J. Biol. Inorg. Chem.* **2008**, *13*, 289.
(6) Pekkanen, A. M.; Mondschein, R. J.; Williams, C. B.; Long, T. E. 3D Printing Polymers with Supramolecular Functionality for Biological Applications. *Biomacromolecules* **2017**, *18*, 2669.
(7) Casini, A.; Woods, B.; Wenzel, M. The Promise of Self-Assembled 3D Supramolecular Coordination Complexes for Biomedical Applications. *lnorg. Chem.* **2017**, *56*, 14715.
(8) Zhang, D.; Ronson, T. K.; Nitschke, J. R. Functional Capsules via Subcomponent Self-Assembly. *Acc. Chem. Res.* **2018**, *51*, 2423.
(9) Brechin, E. K. Using tripodal alcohols to build high-spin molecules and single-molecule magnets. *Chem. Commun.* **2005**, 5141.
(10) Dalgarno, S. J.; Power, N. P.; Atwood, J. L. Metallo-supramolecular capsules. *Coord. Chem. Rev.* **2008**, *252*, 825.
(11) Fox, O. D.; Drew, M. G.; Beer, P. Resorcarene-based nanoarchitectures: metal-directed assembly of a molecular loop and tetrahedron. *Angew. Chem.* **2000**, *112*, 139.
(12) Li, D.; Zhou, W.; Landskron, K.; Sato, S.; Kiely, C. J.; Fujita, M.; Liu, T. Viral-Capsid-Type Vesicle-Like Structures Assembled from $M_{12}L_{24}$ Metal–Organic Hybrid Nanocages. *Angew. Chem. Int. Ed.* **2011**, *50*, 5182.
(13) Perry Iv, J. J.; Perman, J. A.; Zaworotko, M. J. Design and synthesis of metal–organic frameworks using metal–organic polyhedra as supermolecular building blocks. *Chem. Soc. Rev.* **2009**, *38*, 1400.
(14) Ward, M. D.; Hunter, C. A.; Williams, N. H. Coordination Cages Based on Bis (pyrazolylpyridine) Ligands: Structures, Dynamic Behavior, Guest Binding, and Catalysis. *Acc. Chem. Res.* **2018**, *51*, 2073.
(15) Xing, W.-H.; Li, H.-Y.; Dong, X.-Y.; Zang, S.-Q. Robust multifunctional Zr-based metal–organic polyhedra for high proton conductivity and selective CO 2 capture. *J. Mater. Chem. A* **2018**, *6*, 7724.
(16) Bols, P. S.; Anderson, H. L. Template-Directed Synthesis of Molecular Nanorings and Cages. *Acc. Chem. Res.* **2018**, *51*, 2083.
(17) Jansze, S. M.; Severin, K. Clathrochelate Metalloligands in Supramolecular Chemistry and Materials Science. *Acc. Chem. Res.* **2018**, *51*, 2139.
(18) Christou, G.; Gatteschi, D.; Hendrickson, D. N.; Sessoli, R. Single-Molecule Magnets. *MRS Bull* **2011**, *25*, 66.
(19) Manoli, M.; Collins, A.; Parsons, S.; Candini, A.; Evangelisti, M.; Brechin, E. K. Mixed-valent Mn supertetrahedra and planar discs as enhanced magnetic coolers. *J. Am. Chem. Soc.* **2008**, *130*, 11129.
(20) Mitchell, S. G.; Molina, P. I.; Khanra, S.; Miras, H. N.; Prescimone, A.; Cooper, G. J. T.; Winter, R. S.; Brechin, E. K.; Long, D.-L.; Cogdell, R. J.; Cronin, L. A Mixed-Valence Manganese Cubane Trapped by Inequivalent Trilacunary Polyoxometalate Ligands. *Angew. Chem. Int. Ed.* **2011**, *50*, 9154.
(21) Taylor, S. M.; Sanz, S.; McIntosh, R. D.; Beavers, C. M.; Teat, S. J.; Brechin, E. K.; Dalgarno, S. J. p-tert-Butylcalix[8]arene: An Extremely Versatile Platform for Cluster Formation. *Chem. Eur. J.* **2012**, *18*, 16014.
(22) Fong, A.; McCormick, L.; Teat, S. J.; Brechin, E. K.; Dalgarno, S. J. Exploratory studies into 3 d/4 f cluster formation with fully bridge-substituted calix [4] arenes. *Supramol. Chem.* **2018**, *30*, 504.
(23) Morita, T.; Damjanović, M.; Katoh, K.; Kitagawa, Y.; Yasuda, N.; Lan, Y.; Wernsdorfer, W.; Breedlove, B. K.; Enders, M.; Yamashita, M. Comparison of the Magnetic Anisotropy and Spin Relaxation Phenomenon of Dinuclear Terbium(III) Phthalocyaninato Single-Molecule Magnets Using the Geometric Spin Arrangement. *J. Am. Chem. Soc.* **2018**, *140*, 2995.
(24) Amolegbe, S. Supramolecular architectures self-assembled using long chain alkylated spin crossover cobalt (II) compounds. *Chem. Commun.* **2017**, *53*, 4685.
(25) Atwood, J. L.; Brechin, E. K.; Dalgarno, S. J.; Inglis, R.; Jones, L. F.; Mossine, A.; Paterson, M. J.; Power, N. P.; Teat, S. J. Magnetism in metal–organic capsules. *Chem. Commun.* **2010**, *46*, 3484.
(26) Fowler, D. A.; Mossine, A. V.; Beavers, C. M.; Teat, S. J.; Dalgarno, S. J.; Atwood, J. L. Coordination Polymer Chains of Dimeric Pyrogallol[4]arene Capsules. *J. Am. Chem. Soc.* **2011**, *133*, 11069.
(27) Fowler, D. A.; Rathnayake, A. S.; Kennedy, S.; Kumari, H.; Beavers, C. M.; Teat, S. J.; Atwood, J. L. Introducing Defects into Metal-Seamed Nanocapsules Using Mixed Macrocycles. *J. Am. Chem. Soc.* **2013**, *135*, 12184.
(28) Jin, P.; Dalgarno, S. J.; Atwood, J. L. Mixed metal-organic nanocapsules. *Coord. Chem. Rev.* **2010**, *254*, 1760.
(29) Jin, P.; Dalgarno, S. J.; Warren, J. E.; Teat, S. J.; Atwood, J. L. Enhanced control over metal composition in mixed Ga/Zn and Ga/Cu coordinated pyrogallol[4]arene nanocapsules. *Chem. Commun.* **2009**, 3348.
(30) McKinlay, R. M.; Cave, G. W. V.; Atwood, J. L. Supramolecular blueprint approach to metal-coordinated capsules. *Proc. Natl. Acad. Sci. U.S.A.* **2005**, *102*, 5944.
(31) Power, N. P.; Dalgarno, S. J.; Atwood, J. L. Robust and stable pyrogallol[4]arene molecular capsules facilitated via an octanuclear zinc coordination belt. *New J. Chem.* **2007**, *31*, 17.
(32) Dalgarno, S. J.; Power, N. P.; Atwood, J. L. Ionic dimeric pyrogallol[4]arene capsules. *Chem. Commun.* **2007**, 3447.
(33) Rathnayake, A. S.; Fraser, H. W. L.; Brechin, E. K.; Dalgarno, S. J.; Baumeister, J. E.; Rungthanaphatsophon, P.; Walensky, J. R.; Barnes, C. L.; Atwood, J. L. Oxidation State Distributions Provide Insight into Parameters Directing the Assembly of Metal–Organic Nanocapsules. *J. Am. Chem. Soc.* **2018**, *140*, 13022.
(34) Rathnayake, A. S.; Fraser, H. W. L.; Brechin, E. K.; Dalgarno, S. J.; Baumeister, J. E.; White, J.; Rungthanaphatsophon, P.; Walensky, J. R.; Barnes, C. L.; Teat, S. J.; Atwood, J. L. In situ redox reactions facilitate the assembly of a mixed-valence metal-organic nanocapsule. *Nat. Commun.* **2018**, *9*, 2119.
(35) Brown, I.; Altermatt, D. Bond-valence parameters obtained from a systematic analysis of the inorganic crystal structure database. *Acta Cryst. B* **1985**, *41*, 244.
(36) Bedford, R. B.; Bruce, D. W.; Frost, R. M.; Goodby, J. W.; Hird, M. Iron (III) salen-type catalysts for the cross-coupling of aryl Grignards with alkyl halides bearing β-hydrogens. *Chem. Commun.* **2004**, 2822.
(37) Bryliakov, K. P.; Talsi, E. P. Evidence for the Formation of an Iodosylbenzene (salen) iron Active Intermediate in a (Salen) iron (III)-Catalyzed Asymmetric Sulfide Oxidation. *Angew. Chem.* **2004**, *116*, 5340.
(38) Solari, E.; Corazza, F.; Floriani, C.; Chiesi-Villa, A.; Guastini, C. Polydentate ligand exchange via formation of a dimetallic complex. Crystal structures of [(thf)Fe(acen) MCl_2](M= Fe or Zn),[ClFe(salphen)FeCl $(thf)_2$],[Ti (acen)$(thf)_2$][$CoCl_3$ (thf)], and [Ti (acen)$(thf)_2]_2$ [Fe_3Cl_8 $(thf)_2$] [acen= *N, N′*-ethylenebis (acetylacetoneiminate), salphen= *N, N′*-o-phenylenebis (salicylideneiminate), and thf= tetrahydrofuran]. *J. Chem. Soc., Dalton Trans.* **1990**, 1345.
(39) Rathnayake, A. S.; Feaster, K. A.; White, J.; Barnes, C. L.; Teat, S. J.; Atwood, J. L. Investigating Reaction Conditions To Control the Self-Assembly of Cobalt-Seamed Nanocapsules. *Cryst. Growth Des.* **2016**, *16*, 3562.
(40) Li, Q.; Luo, T.-Y.; Taylor, M. G.; Wang, S.; Zhu, X.; Song, Y.; Mpourmpakis, G.; Rosi, N. L.; Jin, R. Molecular "surgery" on a 23-gold-atom nanoparticle. *Sci. Adv.* **2017**, *3*, e1603193.
(41) Wang, Z.-Y.; Wang, M.-Q.; Li, Y.-L.; Luo, P.; Jia, T.-T.; Huang, R.-W.; Zang, S.-Q.; Mak, T. C. Atomically precise site-specific tailoring and directional assembly of superatomic silver nanoclusters. *J. Am. Chem. Soc.* **2018**, *140*, 1069.
(42) Li, S.; Du, X.-S.; Li, B.; Wang, J.-Y.; Li, G.-P.; Gao, G.-G.; Zang, S.-Q. Atom-precise modification of silver (I) thiolate cluster by shell ligand substitution: a new approach to generation of cluster functionality and chirality. *J. Am. Chem. Soc.* **2018**, *140*, 594.
(43) Kato, F.; Kittilstved, K. R. Site-Specific Doping of Mn^{2+} in a CdS-Based Molecular Cluster. *Chem. Mater.* **2018**, *30*, 4720.
(44) Winpenny, R. E. P. Serendipitous assembly of polynuclear cage compounds. *J. Chem. Soc., Dalton Trans.* **2002**, 1.

(45) Pastoriza-Santos, I.; Liz-Marzán, L. M. *N,N*-Dimethylformamide as a Reaction Medium for Metal Nanoparticle Synthesis. *Adv. Funct. Mater.* **2009**, *19*, 679.
(46) Pastoriza-Santos, I.; Liz-Marzán, L. M. Formation and Stabilization of Silver Nanoparticles through Reduction by *N,N*-Dimethylformamide. *Langmuir* **1999**, *15*, 948.
(47) Pastoriza-Santos, I.; Liz-Marzán, L. M. Synthesis of Silver Nanoprisms in DMF. *Nano Lett.* **2002**, *2*, 903.
(48) Gao, G.-Q.; Xu, A.-W. Efficient catalytic reduction of azo dyes by N, N-dimethylformamide mediated by viologen. *New J. Chem.* **2014**, *38*, 4661.
(49) de Groot, M. T.; Koper, M. T. M. Redox transitions of chromium, manganese, iron, cobalt and nickel protoporphyrins in aqueous solution. *Phys. Chem. Chem. Phys.* **2008**, *10*, 1023.
(50) Neves, A.; de Brito, M. A.; Vencato, I.; Drago, V.; Griesar, K.; Haase, W. $Fe^{III}Fe^{III}$ and $Fe^{II}Fe^{III}$ Complexes as Synthetic Analogues for the Oxidized and Reduced Forms of Purple Acid Phosphatases. *lnorg. Chem.* **1996**, *35*, 2360.
(51) Caneschi, A.; Cornia, A.; Lippard, S. J.; Papaefthymiou, G. C.; Sessoli, R. Magnetic properties of dodecanuclear mixed valence iron clusters. *Inorg. Chim. Acta.* **1996**, *243*, 295.
(52) Papadaki, I.; Malliakas, C. D.; Bakas, T.; Trikalitis, P. N. Molecular Supertetrahedron Decorated with Exposed Sulfonate Groups Built from Mixed-Valence Tetranuclear Fe_3^{3+} Fe^{2+} $(\mu_3\text{-}O)(\mu_3\text{-}SO_4)_3$ $(-CO_2)_3$ Clusters. *lnorg. Chem.* **2009**, *48*, 9968.

Insert Table of Contents artwork here